Detecting periodic time scales of changes in temporal networks

Elsa Andres[1], Alain Barrat[2] and Márton Karsai[1,3,†]

[1]*Department of Network and Data Science, Central European University, Quellenstraße 51, Vienna 1100, Austria*
[2]*Aix Marseille Univ., Université de Toulon, CNRS, CPT, Turing Center for Living Systems, 163 avenue de Luminy, Marseille 13288, France*
[3]*National Laboratory for Health Security, Alfréd Rényi Institute of Mathematics, Reáltanoda utca 13-15, Budapest 1053, Hungary*
[†]Corresponding author. Email: Email: karsaim@ceu.edu

Temporal networks are commonly used to represent dynamical complex systems like social networks, simultaneous firing of neurons, human mobility or public transportation. Their dynamics may evolve on multiple time scales characterizing for instance periodic activity patterns or structural changes. The detection of these time scales can be challenging from the direct observation of simple dynamical network properties like the activity of nodes or the density of links. Here, we propose two new methods, which rely on already established static representations of temporal networks, namely supra-adjacency and temporal event graphs. We define dissimilarity metrics extracted from these representations and compute their power spectra from their Fourier transforms to effectively identify dominant periodic time scales characterizing the changes of the temporal network. We demonstrate our methods using synthetic and real-world data sets describing various kinds of temporal networks. We find that while in all cases the two methods outperform the reference measures, the supra-adjacency-based method identifies more easily periodic changes in network density, while the temporal event graph-based method is better suited to detect periodic changes in the group structure of the network. Our methodology may provide insights into different phenomena occurring at multiple time scales in systems represented by temporal networks.

Keywords: temporal networks, power spectrum

1. Introduction

Many complex systems, commonly described as networks, are evolving dynamically as their elements and the interactions between them are subject to changes in time. The recent availability of temporally resolved network data sets has stimulated the emergence of the new field of temporal networks [1–3], which has been useful to describe a wide range of phenomena, from human behaviour [4–6] to biological and ecological systems [7, 8] or public transportation [9, 10]. The temporal network representation provides an effective tool to investigate the structure and dynamics of these systems, as well as the potential dynamical processes occurring on top of them [1, 11]. In particular, this representation goes beyond the conventional static description of networks [12], as it keeps track of the temporal order of successive interactions between elements. This allows for instance to identify notions of potential causality through the definition of temporal paths between nodes, that is, series of successive interactions along which information can be transmitted [13, 14].

Temporal networks present different time-dependent properties at different structural scales. For instance, single nodes can be characterized by their instantaneous degree (number of neighbours at a given time) or other instantaneous centrality measures, which may vary as a function of time [3, 12, 15, 16].

Links are also temporal objects: connections between nodes appear and disappear, often following bursty and correlated dynamics, as well as circadian patterns, which are all typical of human dynamics [17–19]. At mesoscopic scales, temporal networks can exhibit temporal motifs [20–22], communities [23], core–periphery [24, 25] or other cohesive structures and hierarchies [26, 27]. These various dynamical properties may evolve at different time scales [28], including overall changes between global states at the macroscopic level [25, 29, 30]. In particular, periodic variations can emerge, for example, driven by the circadian fluctuations of human behaviour [19, 31], regular scheduling in different contexts like in transportation or schools, or the repetition of metabolic reactions in biological systems [32]. Interesting relevant examples of such variations are given by changes in the connection density in the network, or in the way nodes form and dissolve groups or communities. For example, the number and structure of social interactions vary due to daily rhythms and schedules in contexts such as workplaces, scheduled social gatherings or in schools, where students interact within a class during lectures, but also with other classes during breaks [31, 33]. The identification of the temporal scales of periodic variations in a temporal network is an important step for the characterization and understanding of the system under investigation. However, their measure represents a challenge as they co-appear with other arbitrary non-periodic temporal scales, which appear as noise and hinder the possibility to detect the periodic behaviour by simply following the temporal evolution of simple network summary measures.

Some recent works have addressed the detection of relevant temporal scales in temporal networks, for example, by optimizing the overlap between the sets of events on consecutive time intervals [34] or by searching for the precise recurrence of connections between nodes in different time windows [35]. Another approach consists in defining the correlation between instantaneous adjacency matrices of the temporal graph [36]. Finally, computing a whole similarity matrix between all pairs of timestamps can make it possible to detect states in which the network structure remains stable [25, 29, 30], but this method requires rather heavy computations.

Here, we contribute to this endeavour by defining a new method to measure the periodic time scales of changes of temporal networks. Given a temporal network as input, we first divide it into temporal sub-networks using successive sliding windows. We then use lossless mappings of these temporal sub-networks to get a sequence of static networks and quantify the dissimilarity between them successively to obtain a dissimilarity function describing the changes between the successive temporal sub-networks. We extract the timescales of this function by computing its power spectrum to identify its main frequencies and harmonics. We focus here on applying this method to the detection of periodic changes in the link density and group structure of temporal networks. To this aim, first we consider synthetic networks in which we impose periodic variations of density and structure with tunable frequencies. We show that the method is able to retrieve the actual time scales of the networks. We then apply our methods on several empirical temporal networks presenting periodic dynamics. In each case, the method captures correctly the system's main characteristic times, which could most often not be extracted by simple measures of the network overall activity. Our work opens the door to a better characterization of the time scales of changes of temporal networks, essential in the understanding of the dynamics of the underlying complex systems.

2. Methods

Let us consider a temporal network $G_T = (V, E_T, T)$ defined as a set V of nodes, and a set E_T of events over a time interval T measured in discrete time: each event $e(i, j, t) \in E_T$ describes a temporal interaction between two nodes $(i, j) \in V \times V$ at a certain time $t \in T$.
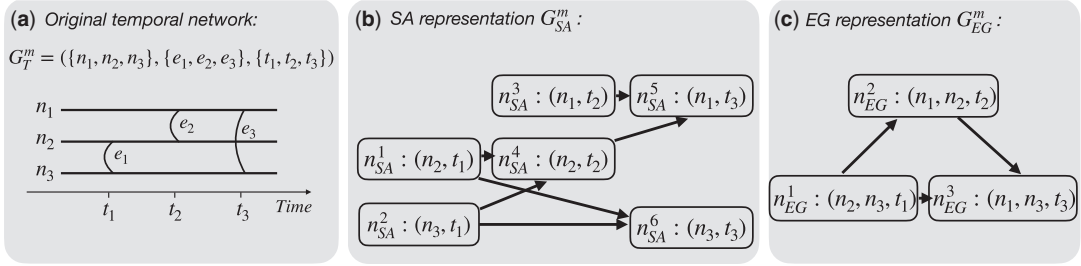
FIG. 1. Example of the representations of a temporal network (a) realized with the Supra-Adjacency (SA) (b) and the Event-Graph (EG) (c) methods. In the original temporal network G_T^m, the time-lines of the nodes are represented by horizontal lines depicting the activity of each node through time (the direction of the time goes from left to right). Each event occurring between two nodes is symbolized by a line linking those two nodes at the corresponding time. The SA and EG representations are static directed networks. In the SA case, the nodes are pairs (node,timestep) of the temporal network. In the EG, the nodes are events, that is, triplets (node,node,timestep) of the temporal network.

Temporal sub-networks.

With such a temporal network as an input, we first extract a sequence of temporal sub-networks of G_T by using sliding windows of length Δt_w and stride t_w (shift between the start of successive windows). Successive windows can thus overlap. Specifically, the sub-network G_T^m is composed of the nodes of V and of the subset E_{T^m} of events of E_T taking place in the time interval starting at time $m * t_w$ and ending at $m * t_w + \Delta t_w$:

$$G_T^m = (V, E_{T^m}, T^m = [m * t_w : m * t_w + \Delta t_w]) \quad \text{for} \quad m \in \mathbb{N} \quad \text{and} \quad T^m \subseteq T. \quad (1)$$

Based on this definition, we can obtain a sequence of temporal sub-networks G_T^m to compute a dissimilarity function characterizing the dynamical changes in the structure and the overall activities present in the original temporal network G_T. More precisely, we want to compute the dissimilarity between consecutive temporal sub-networks, G_T^m and G_T^{m+1}. However, while there exist several methods to compare static networks, few exist to quantify the dissimilarity between two temporal networks. We thus choose to map the temporal sub-networks into static network representations in order to use an already known and validated comparison method for static networks [37], that we adapt to our purposes (see next paragraph and Appendix A).

Static network representations.

We thus first map each temporal sub-network onto a static network representation using two different methods described in Fig. 1. Note that both of these representations are lossless and contain the same amount of information as the temporal network they represent (in particular, they have been designed to conveniently encode information on all the temporal paths existing in the original temporal network):

- The *Supra-Adjacency* (SA) representation [38, 39] $G_{SA} = (V_{SA}, E_{SA})$ of a temporal network G_T is a static directed network, in which each node $v_{SA} \in V_{SA}$ represents a pair (node, time) of the original temporal network: the node $(i, t) \in V_{SA}$ denotes that the node $i \in V$ was active at time $t \in T$, that is, had at least one interaction at t. A directed edge $e_{SA} \in E_{SA}$ between two nodes of V_{SA}, (i, t_a) and (j, t_b) (with $t_a < t_b$), encodes the fact that an information can propagate on G_T from node i at t_a to

node j at t_b, without intermediary events. If $i = j$, this is possible if t_a and t_b are successive interaction times for i (there is no event involving i at times $t_a < t < t_b$). Edges of type $(i, t_a) \rightarrow (i, t_b)$ in E_{SA} thus simply correspond to following the successive interaction times of i in G_T. For instance in Fig. 1, node n_2 is involved in the events e_1 and e_2, happening respectively at times t_1 and t_2. As it is the same node in two consecutive events, there is an edge in the SA representation between (n_2, t_1) and (n_2, t_2). For $i \neq j$ instead, the event $(i, j, t_a) \in E_T$ results in two directed edges in E_{SA}: $(i, t_a) \rightarrow (j, t_b)$ and $(j, t_a) \rightarrow (i, t_c)$, where t_b (resp. t_c) is the first time after t_a in which j (resp. i) is active again. In Fig. 1, there is an edge in the SA representation between (n_2, t_1) and (n_3, t_3) and another edge between (n_3, t_1) and (n_2, t_2) as the nodes n_2 and n_3 are linked at time t_1 in the original temporal networks. The direction of edges in G_{SA} respects the arrow of time, and the set of edges E_{SA} allows to preserve the information about all possible temporal paths of the original temporal network.

- The *Event-Graph* (EG) representation G_{EG} [40, 41] is a static weighted directed acyclic network representation of a temporal network. Each event in G_T is represented by a node in G_{EG}, and two nodes of G_{EG} are connected if the two corresponding events in G_T were adjacent [40], that is, share at least one node (in V) and are consecutive. For instance, there is an edge in Fig. 1 between the nodes of the EG representation corresponding to the events e_1 (n_{EG}^1) and e_2 (n_{EG}^2) as they share the node n_2. Each edge between two nodes in G_{EG} is directed along the direction of time (from the earlier event to the later one) and is weighted by the time difference between the two corresponding events. Consequently, G_{EG} encodes also all information of time respecting paths emerging in the original temporal network.

These representations can be applied to any temporal network. In particular, we apply them to each temporal sub-network G_T^m defined above to map them into a sequence of static representations G_{SA}^m and G_{EG}^m. In the following, we use the symbol $*$ to refer to the static representation method: it replaces the abbreviation *SA* or *EG*, as every object from now on can be calculated using one method or the other.

Network dissimilarity function.

As a next step we compute a dissimilarity function $D_*(m)$ between successive static networks, G_*^m and G_*^{m+1}, for each sequence of static representations $\{G_*^m, m = 1, \ldots\}$. To this aim, we consider here an extension of the method of [37] that summarizes the properties of a network in a matrix where the element (k, l) gives the number of nodes that can reach k other nodes in l hops in the structure (see Appendix A for more details). As we originally deal with temporal networks, and as the nodes of the SA and EG representations do keep temporal information, we instead describe each G_*^m by a tensor $B_*^m(j, k, \tau)$, which gives the number of nodes in G_*^m from which one can reach, in two hops on G_*^m, other nodes of G_*^m involving j nodes, k events and τ timestamps of G_T^m. The dissimilarity function D_*^m is finally computed as the Kullback–Leibler divergence between B_*^m and B_*^{m+1}. At that step, we have to ensure that the dissimilarity function respects the Nyquist–Shannon sampling theorem [42], that is, that its sample rate is at least twice bigger than the observation frequency of the temporal network. It is also worth noticing that the method which compares the temporal sub-networks should be asymmetric because it has to be able to differentiate between the transition of the original network from one state to another, from the opposite transition.
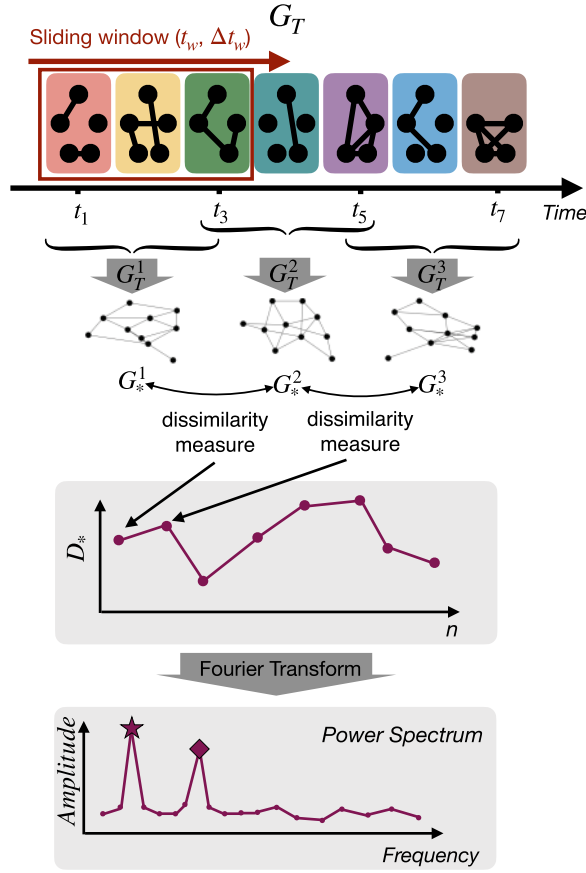
FIG. 2. Methodology pipeline to measure the time scales of changes of a temporal network G_T. From top to bottom: the initial temporal network is divided into sub-temporal networks through a sliding window of parameters t_w (shift between two consecutive windows) and Δt_w (length of the sliding window). The sub-network is denoted G_T^m. A static representation of each sub-network (G_*^m) is generated through the method * (either Supra-Adjacency or Event-Graph). Each G_*^m is then described by a three-dimensional tensor $B_*^m(j, k, \tau)$ that encodes information about the paths and distances in the sub-network (see Appendix A). We compare consecutive tensors with a dissimilarity measure, obtaining the dissimilarity function D_*. Finally, we compute the power spectrum of D_* and measure the frequencies of the main harmonics.

Power spectrum of dissimilarity function.

Each dissimilarity function D_* provides an overall signal that reflects the structural and activity changes in the original temporal network. It presents higher values when the network goes through larger and abrupt transformations and takes smaller values when the network is more stable or changing only gradually with time. It can thus provide insights into the time scales of dynamical changes in the original temporal network. In particular, periodic patterns of network changes can be revealed by taking the power spectrum of the dissimilarity function, which should present harmonics at the characteristic frequencies of the temporal network. More precisely, we compute the magnitude-square of the discrete-time Fourier

transform of D_* defined as:

$$
PS_k = \left| \sum_{j=0}^{N_{\text{sample}}} D_*(j) e^{i2\pi kj/N_{\text{sample}}} \right|^2 , \tag{2}
$$

where N_{sample} is the length of D_* and $k \in [0, N_{\text{sample}} - 1]$. The frequency corresponding to the harmonic PS_k is $f_k = \frac{k}{t_w N_{\text{sample}}}$, where t_w is the time shift between two successive sub-networks G_T^m. The main harmonics of the PS function (appearing as the largest modes in the transformed function) correspond to the principal frequencies of the temporal network. Their inverse yield the characteristic time scales of the main periods present in the network dynamics.

In the following, we refer to the full methodology pipelines using respectively the SA and EG representations as the SA-method and EG-method. The whole generic pipeline is summarized in Fig. 2.

3. Validation on synthetic data sets

To better understand the temporal properties that the above defined dissimilarity functions and their power spectra can capture, we focus on synthetic temporal networks with controlled structural and temporal properties. In particular, we consider networks with tunable changes in activity (number of events per timestamp) and group structure. We utilize the Activity-Driven temporal network (ADN) model [43] for these purposes, defined by a set of N nodes $i = 1, \ldots, N$, each having an intrinsic activity a_i taken from a given distribution. At each time step, node i becomes active with probability ηa_i and, if active, establishes connections with m other nodes chosen randomly. Connections are erased after each time step thus the model does not present any memory nor correlations between time steps. Here, we consider networks of size $N = 100$ with a power-law node activity distribution with minimum value $\varepsilon = 0.001$ and parameters $\gamma = 1.8, m = 4, \eta = 4$ and $| T |= 9200$.

Using these parameters as baseline, we build three types of periodically varying temporal networks, to model the following settings:

- *Change of activity*: we simulate an ADN in which the density of edges varies periodically in time. We assign to each node i two activity values a_i^1 and a_i^2, respectively extracted from two power-law distributions with exponents $\gamma_1 = 1.8$ and $\gamma_2 = 2.8$. We then alternate periodically (and synchronously for all nodes) between the two activity values, with a period T_a. This results in periodic changes in the overall activity of the network, as illustrated in Fig. 3a.

- *Change of grouping*: we consider an ADN model of $N = 100$ nodes forming groups of 5 nodes each, and we periodically alternate, with a period of T_g, between time intervals in which connections are made at random with no restriction as in the baseline and intervals in which only connections within groups are allowed. The average activity is kept constant over time (Fig. 3b).

- *Change of activity and grouping*: finally, we consider an ADN in which both activity and group structure change periodically over time, by combining the previous two mechanisms, each with its own period, respectively T_a and T_g (see Fig. 3c).
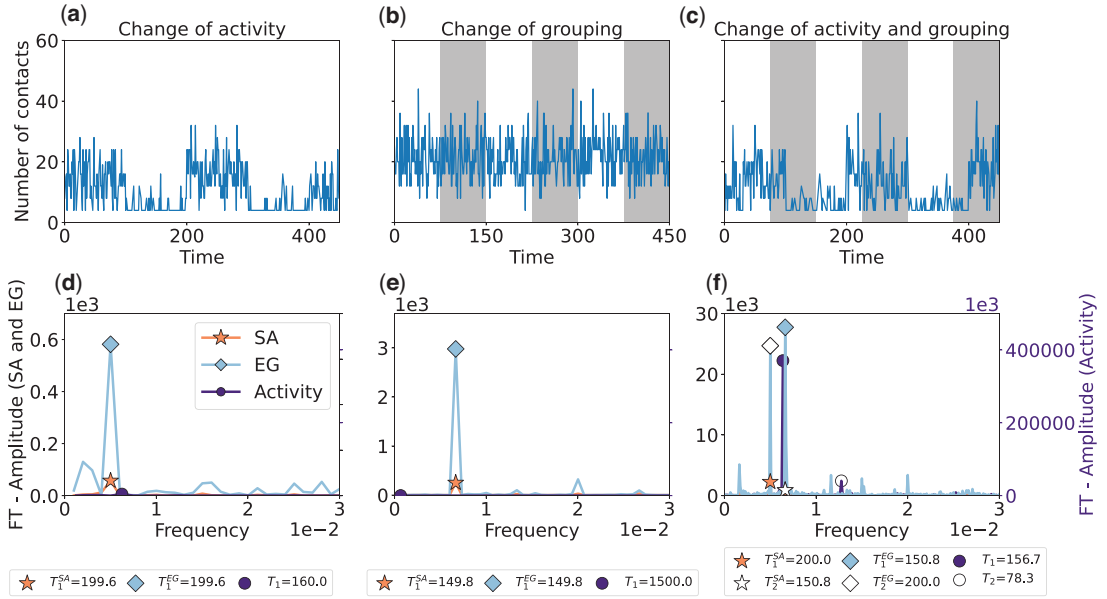
FIG. 3. Schematic representation of three settings simulated with the Activity-Driven temporal network model with periodic changes of parameters ($N = 100$, $\epsilon = 0.001$, $\eta = 4$). (a) The *Change of activity* case presents networks with activity periods of $T_a = 200$; (b) the *Change of grouping* case presents recurrent structural changes with period $T_g = 150$; while (c) the *Change of activity and grouping* setting is defined as a mix of both dynamics. Panels (a-c) display the number of events as a function of time for a realization of each experiment; Gray areas in panels b and c indicate the intervals in which interactions can only occur within groups. Panels (d-f) depict the power spectra of these networks obtained respectively through the SA-method and EG-method, as well as the power spectrum of the activity timeline. The first and second harmonics of each power spectrum are shown respectively with a full symbol and an empty symbol. In each case, the SA-method and EG-method are able to retrieve the correct period of the networks, while the power spectrum of the activity signal fails in measuring temporal structural changes. In the *Change of activity and grouping* case, the SA-method identifies the frequency of activity changes as the main harmonic, while the EG-method detects the structural changes frequency as the dominant one.

For each case, we apply the SA and EG methods to compute the power spectra of the resulting temporal networks. As a baseline method, we compute directly the power spectrum of the activity function, that is measured as the link density at each time step of observation (see Fig. 3). This is a simple summary metrics that describes the overall changes in the temporal network and can be computed for any system.

3.1 Results

The settings we consider involve either one or two types of periodic changes in the synthetic temporal networks: a periodic fluctuation in the amount of activity and/or in the network structure in terms of inter and intra group interactions. Our first goal is to investigate whether the SA- and EG-methods can uncover the corresponding periods T_a and T_g through the measure of the dominant frequencies in the associated power spectrum. As shown in Fig. 3d and e, when only one type of periodic change is present, both methods are able to detect the corresponding period. It is evident from the depicted symbols that indicate the largest mode in the frequency scale, correctly positioned at the right frequency corresponding to the period of the actual periodic changes. At the same time, the baseline method, computed as the *PS* of the activity timeline, strongly underperforms as compared to the other two methods. While in case
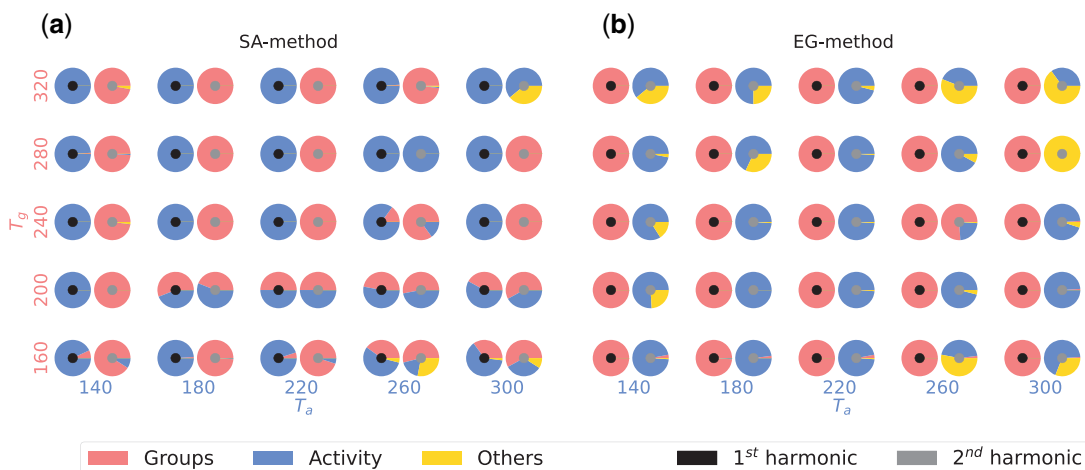
FIG. 4. Periods corresponding to the two first harmonics measured through the SA-method (a) and the EG-method (b), for periodic synthetic temporal networks generated through the *Change of activity and grouping* setting ($N = 100$, $\varepsilon = 0.001$, $\eta = 4$, $\mid T \mid = 9200$) with respective periods T_a (x-axis) and T_g (y-axis). For each pair of values (T_a, T_g), we generate 100 realizations of the temporal network and apply the SA- and EG-method to extract the two main harmonics. We show in blue around a small black disk (resp. grey disk) the fraction of realizations in which the main frequency (resp. the second main) corresponds to T_a, in pink the fraction of cases in which it yields T_g, and in yellow the cases in which it corresponds to neither (we consider a tolerance of 10% for both periods). In most cases, both periods are correctly inferred, with the main frequency corresponding to T_a in the SA-method and to T_g in the EG-method.

of activity changes (see Fig. 3d) it at least identifies approximately the value of the period, in case of periodical group changes it does not succeed to capture the rightful period at all. This was expected as in this case the overall activity does not reflect any periodicity but simply fluctuates randomly around a constant value.

When both types of periodic changes are present, an interesting distinction emerges between the results of the SA- and EG-methods. Indeed, both methods correctly detect the T_a and T_g periods as the first two dominant frequencies in the power spectrum. However, in the SA-method the frequency describing the periodic activity changes is identified as the dominant frequency and the periodic group frequency to the second largest value ($T_1^{SA} = T_a = 200$, $T_2^{SA} = T_g = 150$ in Fig. 3f), while this is reversed for the EG-method ($T_1^{EG} = T_g = 150$, $T_2^{EG} = T_a = 200$ in Fig. 3f). These results suggest that the SA-method is more sensitive to periodic changes in activity, while the EG-method is more suited to detect periodic structural fluctuations. We also note that the PS of the baseline method yields as dominant timescales $T_1 = 156.7$ and $T_2 = 78.3$, the first one describing approximately the activity periods of the network, while the second one does not correspond to the period of either of the underlying processes.

To check the robustness of the proposed methods against the relative values of the periods, we further investigate this point by exploring systems with different values of T_a and T_g in the *Change of activity and grouping* setting. We generate 100 synthetic temporal networks for each pair of values (T_a, T_g), compute the dissimilarity function and power spectra of these realizations, and extract the corresponding first two harmonics for each method (SA and EG).

Figure 4 summarizes the results by showing in each case the fraction of realizations which detected the periods of T_a, T_g correctly, or failed to detect any of them. These results demonstrate again that the SA-method identifies predominantly T_a (the activity change period) through the first harmonic and T_g

(change of group structure) through the second, while the reverse is observed for the EG-method. Some deviations from this behaviour are observed at large values of the periods and/or when T_a and T_g are close to each other.

3.2 *Parameter dependencies and limitations*

Both the synthetic temporal networks and the analysis method involve some parameters. In particular, we explore their dependencies on the network size, temporal length and ratio between total temporal length and periods of changes T_a or T_g, with results presented in Appendix B. We observe that at large network size, both methods identify as main frequency a value corresponding to the half value of the original period. Moreover, evidently, for correct time scale detection the observation period of the temporal network needs to cover at least two full periods of any kind of changes. In addition, regarding the experiment *Change of activity*, both methods are very sensitive to this kind of changes. Even small variations of the density of links through time, obtained by changing the exponent γ of the ADN, are detected.

The first step of our pipeline moreover involves the definition of sliding windows with stride t_w and length Δt_w. Naturally, these parameters affect the amount of information contained in each sub-temporal network and consequently influence the resulting dissimilarity function [44–46]. We explore the effect of these parameters in Appendix B, while keeping $t_w \leq \Delta t_w$ to have a non-zero overlap between successive time windows. We also ensure that the two parameters under study have values below the time span of the network's period (their maximum value is 20 while the period is 100).

As shown in Appendix B in Fig. B.5, the two methods show the best performance if the t_w stride is not too large and if Δt_w length is neither too high nor too small. If the time interval between two temporal sub-networks t_w is too high, we collect less information about the similarity between successive sliding windows. The dissimilarity function is then less precise and our methods perform less well to identify the characteristic temporal scales. Moreover, if Δt_w is too small, each sliding window contains too little information to obtain an accurate measure of the time-scale of the original network. On the opposite, if Δt_w is too large, each temporal sub-network may summarize too much information and loose the specific characteristic of the activity or the structure of the network on a certain time or interval of time. As an observation bias this could smooth dissimilarities between consecutive temporal network slices as they average too much information, and not because the network does not present significant changes through time. It is also worth noticing that both methods measure systematically half of the period as dominant modes for very large values of t_w and Δt_w (Appendix B, Fig. B.5). In that case, every half-period of the network is covered by a small number of temporal sub-networks, leading to a lack of resolution in the dissimilarity function, in which only the peaks of dissimilarity at half-periods are well marked, leading to the detection of the half-period as typical timescale. Another limitation of these methods is that they cannot measure time scales of networks having periods equal to their time resolutions. It is because it is not feasible to create a sliding window capable of detecting the changes, as it should be smaller than the period, which is the time resolution in this case.

4. Applications on real networks

After validating our methods on synthetic networks with controlled properties, to explore further the capabilities of our methods, we consider empirical temporal networks representing different systems. We note that in such systems, in contrast to the cases studied above, several time scales, that correspond both to periodic or non-periodic fluctuations, may co-exist, as well as structural changes of different nature.

4.1 *Data sets*

We consider four temporal networks describing interactions of different nature, with various sizes and over different observation lengths. For more details about their temporal dynamics, see Appendix C.

- *US middle school network*: this data set describes close proximity interactions between students of a middle school in the USA, during 1 day with temporal resolution of 20 s [47], recorded by Radio Frequency Identification (RFID) wearable devices. It involves several periods of class-times and inter-class breaks including two lunch periods, when students freely mix while changing classroom or eating together. The network consists of 591 nodes (each node corresponding to a student) and contains 473, 755 records of pairwise temporal interactions between them.

- *US flight network*: this air-transportation network describes the direct flight connections between 278 airports in the USA [48]. In our observation period, we concentrate on 4 days of data that records 71, 315 flights between the airports that we consider as undirected temporal interactions. This network is expected to show strong periodicities in activity, reflecting the daily recurrent flight schedules, while structural changes may not be strong as almost always the same airports are connected every day.

- *Conference network*: these data also describe face-to-face contacts between individuals, with a temporal resolution of 20 s, obtained from the SocioPatterns collaboration [49] by RFID devices built on a different architecture. The contacts were measured during a scientific conference, namely the IC2S2 conference that took place in Cologne (Germany) in 2017 [50]. Our observation period spans over the three first days of the conference, and records 229,536 temporal contacts between 274 participants. This data set is expected to show periodic behaviour both in terms of activity and structural changes, by reflecting the circadian pattern characterizing the daily life of the participants.

- *Resistance game network*: it is an eye-contact network between participants of the Resistance game [51, 52], which is a role game where some of the players are hidden 'defeaters', and the goal of the other players is to uncover them. The game involves multiple rounds of around 4 min each, starting with a discussion involving every participant, and ending with a vote. The recorded network is built from directed events between participants who looked at each other at a given time *t*. The network is recorded between eight individuals and contains 52,731 temporal interactions that we deem undirected for simplicity. This network provides an example where the interaction level should not reflect strong periodicity but the grouping of participants changes between each session.

4.2 *Results*

After applying our pipeline on each data set using both the SA- and EG- and the baseline methods, in Fig. 5, we depict the power spectra of the obtained dissimilarity functions, with symbols indicating the dominant frequencies. Interestingly, both the SA- and EG-methods identify the relevant timescales of changes in most networks, while the baseline method consistently failed to detect them. For the *US middle school network*, both methods yield a timescale of about 46 min, coherent with the length of a class. Meanwhile, the baseline activity timeline PS would estimate the dominant frequency as corresponding to a period of 139 min. In the case of the *US flight network*, where the main changes are expected to be ruled by circadian fluctuations, both SA- and EG-methods also correctly identified periods of around 24 h. This time-scale is also captured by the baseline method, but recognised only as its third largest harmonic. The two first harmonics are identified as periods of 5 and 10 min, which may correspond to the characteristic times between consecutive departures of planes from the same airport. The *Conference network* also
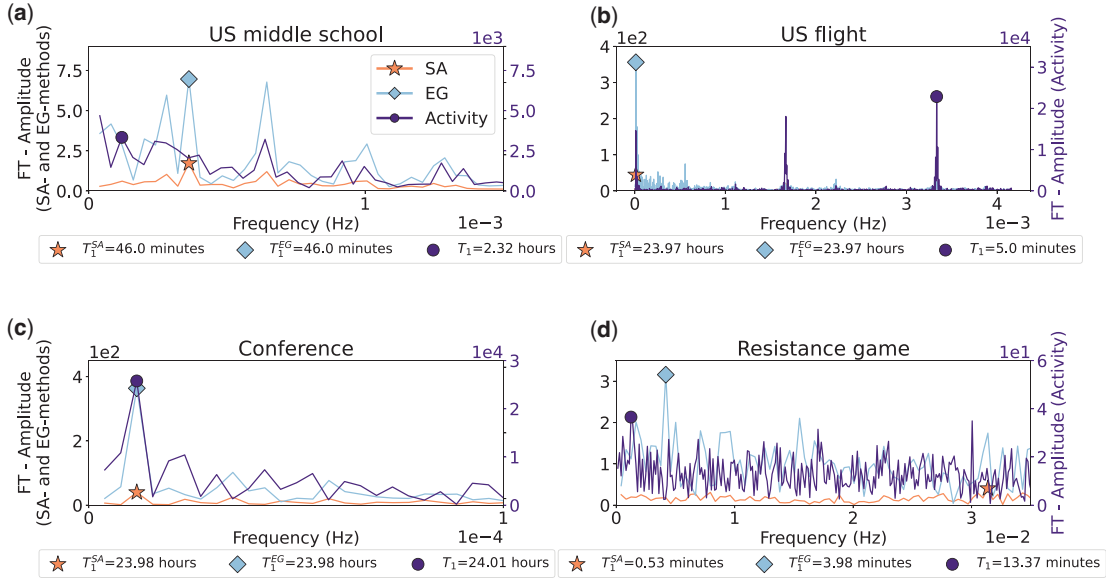
Fig. 5. Power spectra of dissimilarity and activity functions of four real-world data sets (a) a US middle-school, (b) a US flight network, (c) a conference, and (d) a resistance game network. Dissimilarity functions were calculated by the SA-method (in orange with star symbols) and the EG-method (in blue with diamond symbols), while results computed for the baseline model using activity signals are shown in purple with round symbols. The highest harmonics are highlighted with a symbol for each PS, and the corresponding values of the period is indicated below each panel. The parameters of the sliding windows (t_w, Δt_w) are (2 minutes, 5 minutes) for the *US middle school*, (2 minutes, 10 minutes) for the *US flight*, (2 minutes, 5 minutes) for the *Conference* and (1/3 minute, 1 minute) for the *Resistance game*.

presents strong signs of circadian changes of activity. This is reflected by all computed power spectra, which show a harmonic corresponding to a period of about 24 h for both the SA-method and the EG-method, captured as well by the baseline method. Finally, regarding the *Resistance game*, which presents only structural changes, the EG-method measures accurately the time scales of periods characterizing a single round in the game, around 4 min. Since no periodic change of activities characterise this network, both the SA-method (more sensitive to activity changes) and the baseline method fail to identify any meaningful time-scale. The power spectrum of the SA-method suggests the dominant mode to correspond to 0.53 min, while the baseline method detects 13 min.

It is worth noticing that we have used different sliding window parameters for the different data sets: (t_w, Δt_w) are (2 min, 5 min) for the *US middle school*, (2 min, 10 min) for the *US flight*, (2 min, 5 min) for the *Conference* and (1/3 min, 1 min) for the *Resistance game*. It is due to the fact that the temporal characteristics of the networks under study vary a lot: from the order of magnitude of the minute for the *Resistance game* to the daily pattern of the *Conference*. The parameters t_w and Δt_w should be chosen in an appropriate manner with respect to the data set and its characteristic time scales, if an a priori knowledge of their order of magnitude is available (cf paragraph 3.2). If it is not possible to know a priori which range of parameters to use according to the data set, one should investigate a spectrum of potential parameters and check that the extracted timescale is robust on a range of parameter values (cf Appendix D).

4.3 *Shuffling of the data*

Empirical temporal network data entail structural and temporal correlations of different nature. To explore which of their characteristics play the main role in determining their relevant time scales, a common

method consists in shuffling the data to create randomized reference models [53] in which specific correlations are destroyed while others are preserved. In other words, through shuffling we create a sample from a uniformly sampled microcanonical ensemble of randomized networks, where certain network properties are kept constrained, while the networks are maximally random otherwise. Specifically, here we consider shuffling methods that remove the periodicity of the activity and/or of the group structure. In turn, we apply the SA- and EG-methods to compute the power spectra of the shuffled data and check how these methods capture the modification of the time scales due to shuffling. We consider the following random reference models, following the canonical notations introduced in [53]:

- $P_p(\Gamma)$ shuffling: To remove both activity and structural correlations, we randomly shuffle the order of the temporal network snapshots, keeping fixed the structure of each snapshot. This procedure destroys any structural correlations between consecutive snapshots, removing the effects of structural reorganizations and randomizing also the activity timeline.

- P_τ shuffling: We rewire randomly all links in each snapshot of the temporal network. This is equivalent to creating a configuration random network [54] in each snapshot, with the same number of nodes and edges as the original snapshot. The activity timeline is thus preserved while the group structure and its changes are removed.

Results are shown in Fig. 6 for the four data sets and the two shuffling procedures. When the networks are shuffled with the $P_p(\Gamma)$ procedure (a–d), the original periods of changes are not recovered, which is expected since the shuffling destroys any periodicity in the data.

However, when we shuffle the networks using the P_τ method, which removes the structural effects but keeps the fluctuations in the overall activity, our methods present some capacity to identify the residual time scales of changes in some of the data sets. In particular, two of the data sets present large periodic activity variations, that is, the *US flight* and the *Conference* networks. After shuffling, these regular changes are still present, as the P_τ method preserves their activity time lines, while any other pattern has been destroyed by the shuffling. Consequently, we may still measure their original circadian period from their P_τ-shuffled versions. Indeed, both the SA- and the EG-methods applied to the *Conference* network recover the dominant time scales, while in case of the *US flight* data set, the EG-method captures the expected time scale of around one day. We also find a time scale of 5 min with the SA-method applied to the *US flight* data set, which corresponds to another characteristic times of activity of this network (see Fig. 5).

In contrast, both the SA- and the EG-methods miss the identification of the original time scales when applied on the P_τ-shuffled *Resistance game*. Since the original network has no periodic fluctuations in terms of activity, its shuffled counterpart does not present either any regular changes in term of activity. Thus, the detected time scales are only induced by some noise in the data.

Finally, the *US middle school* network presents activity variations that are not easily assessed even in the original network. Once shuffling with the P_τ method, only the SA-method, which is overall more sensitive to activity changes, retrieves the original period (≈ 46 min) in the shuffled network. The EG-method overestimates this time by detecting a period of ≈ 59 min.

5. Conclusion

In this work, we have put forward a new methodology to uncover periodic time scales of changes in temporal networks. In our proposed pipeline, first we locally aggregate the original temporal network by using a sliding window to build a sequence of temporal sub-networks. Subsequently, we map these
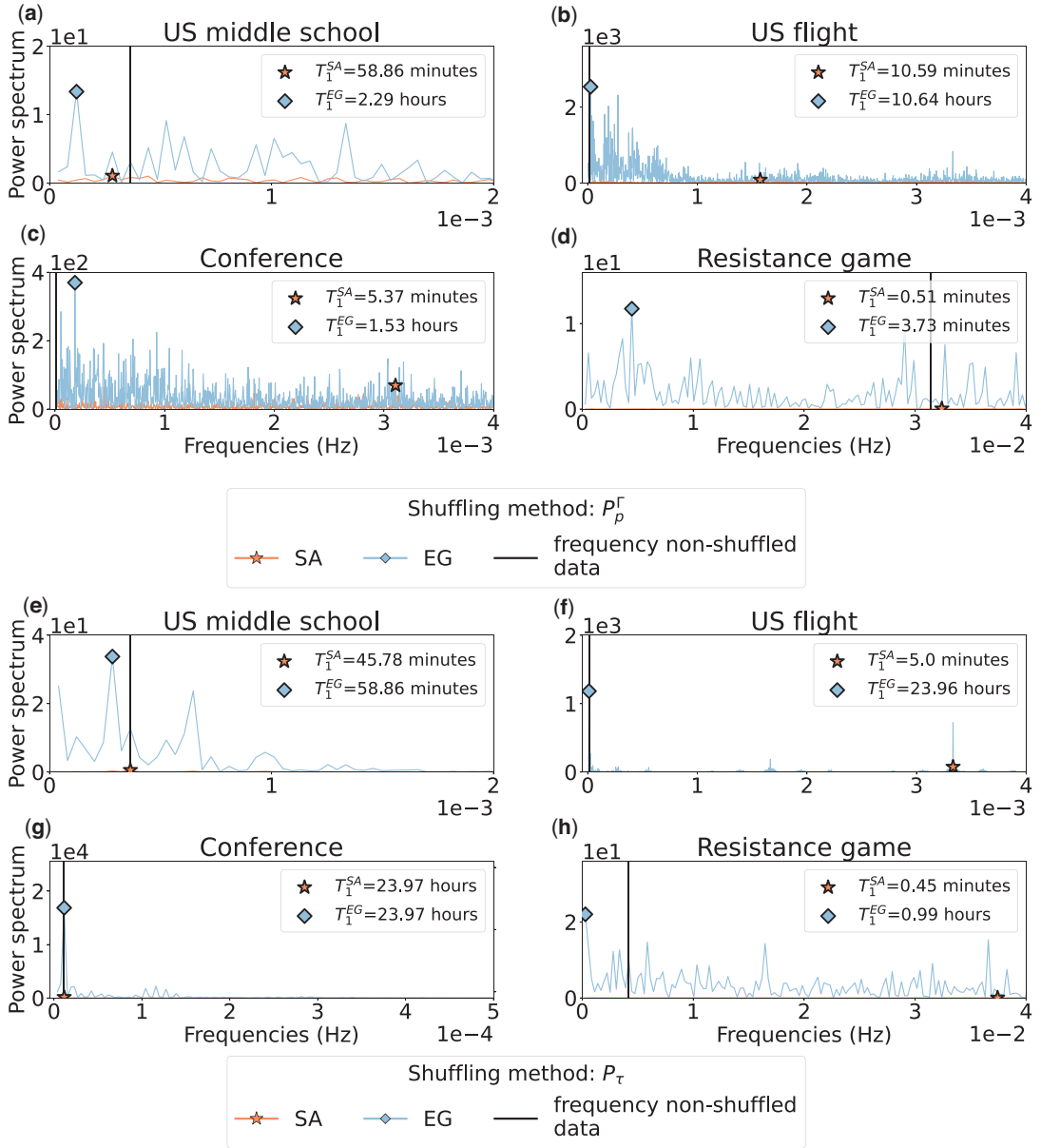
FIG. 6. Power spectra for the data sets *US school*, *US flight*, *Conference* and *Resistance game* networks shuffled using the two shuffling methods $P_p(\Gamma)$ (panels a-d) and P_t (panels e-h), obtained with the SA-method (orange curve with star symbols) and the EG-method (blue curve with diamond symbols). The period of each original data set is indicated with a black vertical line. For data shuffled using the $P_p(\Gamma)$ method, the original period is never recovered. In the case of the P_t shuffling instead, the SA- and EG methods still measure original periods if the network presents large activity changes (*US flight* and *Conference* data sets). In the case of the *US middle school* network, only the SA-method is able to assess the original time scale as this method performs better to detect activity changes. Finally, none of the method can measure the original period of the *Resistance game* network shuffled with the P_t method as it does not present any periodic variations.

temporal sub-networks into a sequence of static networks, using known lossless higher-order temporal network representations, namely supra-adjacency matrices or event-graphs. We further extend a method for the comparison between the consecutive static network samples to define a dissimilarity function that reflects activity and structural changes in the original temporal network. Finally, we take the power spectrum of the dissimilarity function to detect the relevant periodic time scales from the dominant frequencies characterizing the original network.

We have explored this pipeline, focusing on changes in the activity and group structure of temporal networks. Using synthetic data sets with prescribed changes, we have shown that while both methods are able to recover the time scales of the modelled periodic dynamics, they perform differently in the identification of changes in activity and structure. Specifically, the SA-method is more sensitive to overall activity changes while the EG-method captures better periodic structural fluctuations, which cannot instead be obtained through the power spectrum of the activity timeline. We have also shown that these methods are able to highlight relevant periods in more complex empirical data sets.

The methodology presented here have certain limitations. First, its performance depends on some parameters of the aggregation method and the temporal network observed. The observation needs in particular to span a long enough interval: at least two periods of changes need to be observed. The sliding window parameters also have some impact on the performance: each temporal sub-network should encode enough information but should not be too long to average out relevant changes. The stride should be small enough to keep a reasonable temporal resolution and a substantial overlap between successive windows. Also, the methods presented in this article cannot measure temporal changes if they are smaller or equal to the time of resolution of the network. Overall, if no prior external knowledge is available on the expected order of magnitude of the network timescales, the method should be tested on a range of parameter values, and the robustness of the extracted timescale should be checked.

The proposed methodology pipeline opens the door to the investigation of several interesting extensions and research questions. Possible extensions of the present method could include the consideration of other static representations as well as other similarity measures between successive temporal sub-networks[1], which could potentially be more sensitive to various types of structural changes of the temporal network. For instance, it would be interesting to explore whether changes in the instantaneous core–periphery structure [25] could be uncovered. Future work could also explore extensions to time-varying hypergraphs [55, 56] or the interaction between the detected time scales of the underlying temporal network and ongoing dynamical processes. Our work presents a proof of concept for a new methodological direction that will contribute to the better characterization of time varying complex structures.

Acknowledgements

---

[1] including the tensor portrait defined in Appendix A but considering different numbers of hops from each node.

Appendix

A. Comparing temporal networks

An important step in our methodology is to quantify the similarity between successive temporal sub-networks. We first map each temporal sub-network to a static one, as described in the main text, and compare these static representations. To this aim, we adapt a method proposed by Bagrow and Bollt [37], which allows to compare static networks at multiple scales. The first step of this method is to compute, for each static network, its "portrait" B defined as

$$B_{l,k} = \text{number of nodes which have } k \text{ nodes at distance } l.$$

The dissimilarity between two networks is then given by the Kullback–Leibler divergence between their respective portraits.

In our case, the static networks that we need to compare are representations of temporal networks, with either the Supra-Adjacency or the Event-Graph method, noted G_*^m. Nodes and edges in these networks contain information about nodes, interactions and times of the original temporal network. To take this into account, we adapt and modify the definition of network portrait, and define the tensor portrait of G_*^m by relying on $BD_*^m(j,k,\tau)$ which is the number of nodes of G_*^m which can reach, in two hops, j nodes, k events and τ timestamps of the original temporal network. In other words, we consider for each node of the static representation G_*^m its ego-network at distance 2, and count the number of distinct nodes,
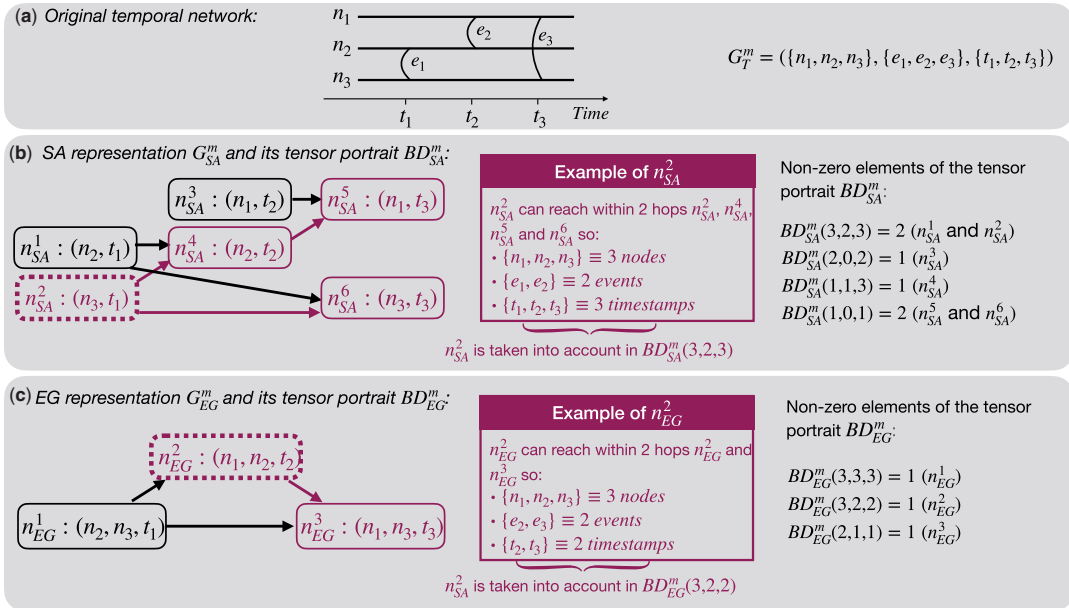

FIG. A.1. Sketch of the method to compute the tensor portraits BD_*^m of the temporal network G_T^m displayed in (a). The static SA and EG representations G_{SA}^m and G_{EG}^m are shown respectively in (b) and (c). We first evaluate the number of nodes, events and timestamps from the temporal network accessible within two hops from each node of the static networks. We illustrate the computation for n_*^2 (purple dashed highlight). We then count the number of nodes of the static representation that can reach j nodes, k events and τ timestamps of the original temporal network to compute the element $BD_*^m(j,k,\tau)$ of the tensor portrait.

timestamps and events of the original temporal network G_T^m involved. We then collect this information for all nodes of G_*^m and summarize the resulting histogram as the portrait BD_*^m. We illustrate this method to compute the tensor portrait BD_*^m in Fig. A.1.

We also note that the static representation of the temporal networks are directed, with edge directions following the arrow of time. The ego-network of a node of the static representation involves only future timestamps and events. To take also into account how each node can receive information from events in the past, we create for each G_*^m its reversed version $G_{*,R}^m$ by inverting the direction of each edge of the representation and compute its portrait BR_*^m. We then obtain the final tensor B_*^m by summing BD_*^m and BR_*^m.

Finally, we compute the dissimilarity between each pair of consecutive tensors B_*^m and B_*^{m+1}, as their Kullback–Leibler divergence (if the two tensors B_*^m and B_*^{m+1} differ in size, we adjust the size of the smaller one to the size of the biggest one by filling the missing entries with zeros). The dissimilarity function is defined as:

$$D_*(m) = KL(B_*^m, B_*^{m+1}) \quad \text{for} \quad m \in \mathbb{N}$$

Note that, in the event of an empty network, the Kullback–Leibler divergence is not defined. We then assign one single event to the corresponding empty temporal sub-network G_T^m.

B. Sensitivity analysis: size and length of the temporal network, sliding window parameters

To evaluate the reliability of our results, we perform a sensitivity analysis on the parameters of the experiments *Change of activity* and *Change of grouping*. We change one parameter in both experiments while keeping the other constant ($N = 100$, $\varepsilon = 0.001$, $\eta = 45$, μ oscillating between 1.8 and 2.8 for the *Change of activity* and $\mu = 2.8$ for *Change of grouping*, $T_a = T_g = 100$, $| T |$ is adjusted to have 12 periods, $\Delta t_w = 5$ and $t_w = 2$).

When we vary the number of nodes of the networks (Fig. B.1), the original period is almost always measured properly except when the number of nodes is high. In that case, the measured period is 50 (corresponding to a frequency of 0.02), which is half of the original period. In fact, when the networks change from a high-activity state to a low-activity state, we observe a peak in the dissimilarity function. This situation happens twice in a period: when changing from low to high and from high to low activity. The measured period is then the half period (Note that this happens at all sizes, and the half-period is indeed always recovered as one of the harmonics, but it seems here to become dominant at large sizes).

The same analysis has been realized by changing the length of the period (Fig. B.2) and in every case, the original period is correctly measured: the length of the period does not influence the observation. Instead, when we change the number of periods observed (Fig. B.3), we observe that we need a minimum of two periods to measure the original time scale. Also, by diminishing the activity difference in the *Change of activity* experiment, by turning the exponents of the activity distribution (Fig. B.4), we show that our methods can detect very small variations of activity. Namely, it can effectively distinguish between variations if the difference between the exponents corresponding to low and high activity is higher than 0.2 for the EG-method and 0.4 for the SA-method.

We finally study the influence of the parameters of the sliding window t_w and Δt_w on the results. In Fig. B.5, we compute the power spectra of the AD network with the SA-method and the EG-method having different parameters t_w and Δt_w. Indeed, in the case of empirical data sets, if no prior information is available on the orders of magnitude, one should explore a range of possible parameters and check the robustness of the extracted timescales. The correct period (100) is properly measured if t_w is not too large and if Δt_w has an intermediate value.
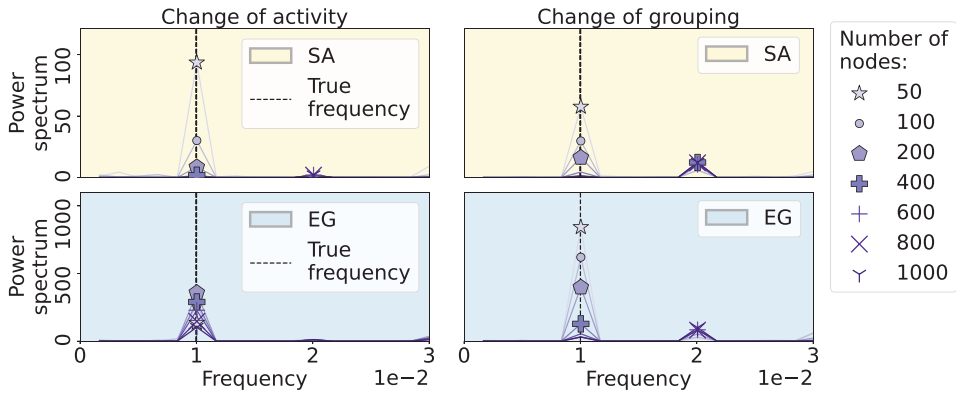
FIG. B.1. Power spectra of the temporal network from the *Change of activity* experiment (left column) and the *Change of grouping* experiment (right column) measured from the SA-method (first row, yellow background) and the EG-method (second row, blue background). The number of nodes of the AD networks varies from 50 to 1000. The correct frequencies are indicated with vertical dashed lines. Those original periods are well-measured in the majority of the cases. However, when the number of nodes is too important, the method measures the semi-period.
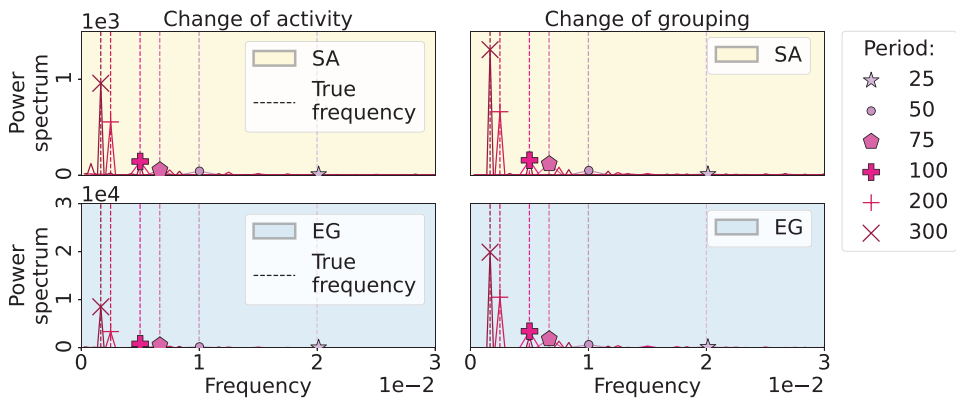

FIG. B.2. Power spectra of the temporal network from the *Change of activity* experiment (left column) and the *Change of grouping* experiment (right column) measured from the SA-method (first row, yellow background) and the EG-method (second row, blue background). The period varies from 25 to 300. The correct frequencies are indicated with vertical dashed lines and are here always well recovered.
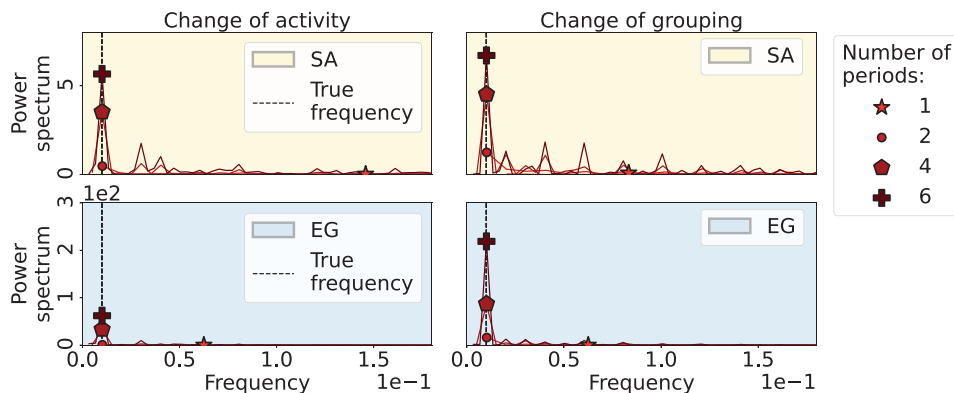
Fig. B.3. Power spectra of the temporal network from the *Change of activity* experiment (left column) and the *Change of grouping* experiment (right column) measured from the SA-method (first row, yellow background) and the EG-method (second row, blue background). The number of periods of the AD networks observed during T varies from 1 to 6. The correct frequencies are indicated with vertical dashed lines. Those proper periods are well-measured as long as the data set contains at least two periods.
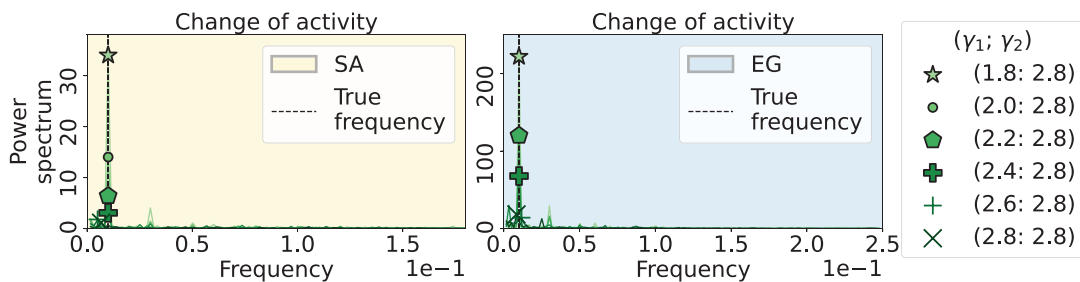

Fig. B.4. Power spectra of the temporal network from the *Change of activity* experiment measured from the SA-method (left column, yellow background) and the EG-method (right column, blue background). The parameter γ_1 of the AD networks corresponding to periods of high activity varies from 1.8 to 2.8, while the other parameter γ_2 characterizing the low-activity state remains constant equal to 2.8. The correct frequencies are indicated with vertical dashed lines. Those proper periods are well-measured as long as γ_1 is different than γ_2.
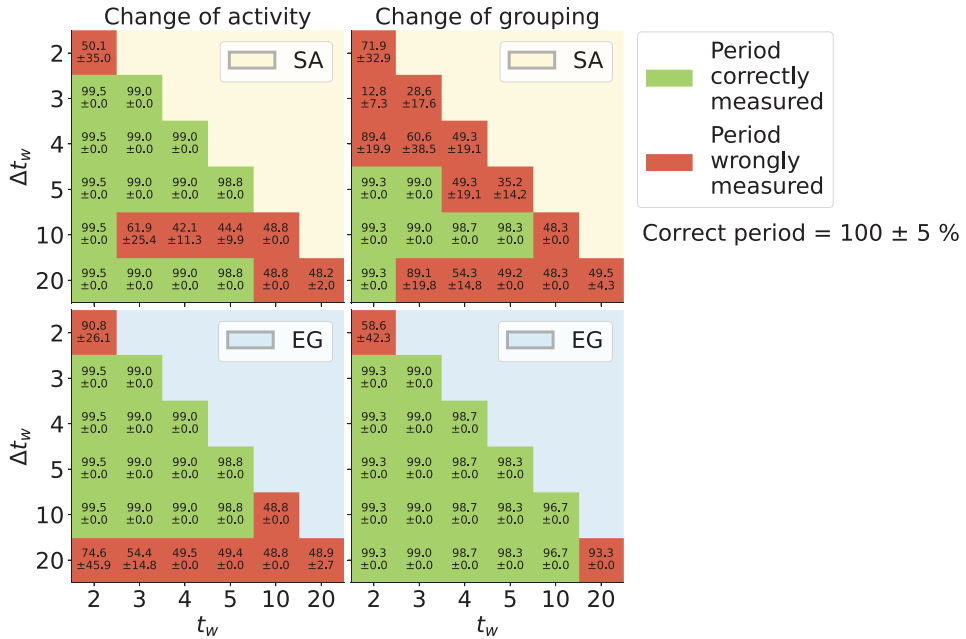
FIG. B.5. Period measured through the SA-method (first row, orange background) and the EG-method (second row, blue background) for the *Change of activity* experiment (first column) and the *Change of grouping* experiment (second column). We change the parameters of the sliding window: the x-axis presents different values of the stride t_w and the y-axis different values of time-window lengths (Δt_w). The period of the initial networks is 100 and the results are averaged over 10 realisations. The results are displayed as the average period over the different realisations $\pm$ the standard deviation.

C. Empirical data

We observe the changes of activity over time of the empirical networks for the four data sets (Fig. C.1). The *US school* presents periodic patterns, varying from low contact periods when the students are in class to high contact periods when there is a recreational time. The *US flight* and *Conference* networks have circadian patterns as there are respectively less flights and less contacts at night. Finally, the *Resistance game* does not present any periodic change in its activity as every player of the game is looking at someone else at each time step.
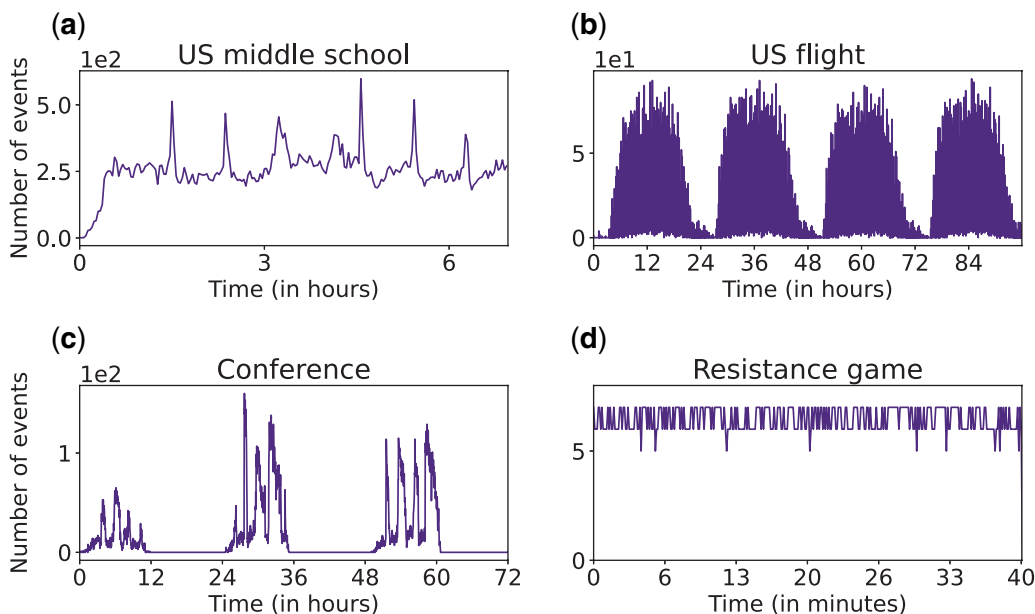
FIG. C.1. Number of events as a function of time for the four data sets: the *US school* (a), the *US flight* (b), the *Conference* (c) and the *Resistance game* (d). The *US school* network contains high activity periods during recreational moments of the students' day, while the *US flight* and the *Conference* networks present circadian patterns. The Resistance game network does not have particular periodic activity changes.
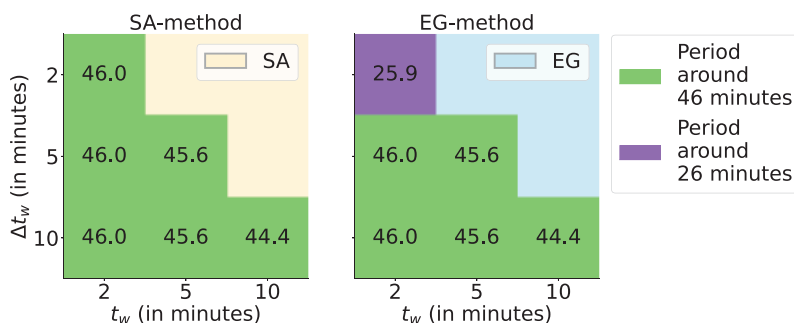

FIG. D.1. Measures of the time scales of changes of the *US middle school* temporal network with the SA-method (left panel) and the EG-method (right panel) for different parameters $(t_w, \Delta t_w)$. The measure of 46 min is robust over the parameter pairs $(t_w, \Delta t_w)$.

D. Choice of the parameters $(t_w, \Delta t_w)$

If one has prior knowledge of the order of magnitude of the time scale of the temporal network under study, the parameters t_w and Δt_w should be selected in a manner that is suitable for the data set and its characteristic time scales. Indeed, Δt_w must be chosen large enough to avoid noise in the measure and small enough to avoid a flattening of the dissimilarity function. Also, the parameter t_w must respect the Nyquist–Shannon theorem (cf paragraphs 2 and 3.2).

If it is not the case, one should explore several parametrizations $(t_w, \Delta t_w)$ and check that the measured time scale is robust over a spectrum of parameter values. This has been proceeded for example on the data set *US middle school* (cf Fig. D.1) and the same period of 46 min is obtained for most of the parameter pairs $(t_w, \Delta t_w)$. The only different value appears when the parameter $\Delta t_w =$ 2 min with the *EG-method*. This is because when the sub-networks are too short, the noise perturbs the measure.

References

1. HOLME, P. & SARAMÄKI, J. (2012) Temporal networks. *Phys. Rep.*, **519**, 97–125.
2. HOLME, P. (2015) Modern temporal network theory: a colloquium. *Eur. Phys. J. B*, **88**, 1–30.
3. MASUDA, N. & LAMBIOTTE, R. (2016) *A Guide to Temporal Networks*. Wuhan, China: World Scientific.
4. BARRAT, A. & CATTUTO, C. (2013) Temporal networks of face-to-face human interactions. *Temporal Netw.*, **40408**, 191–216.
5. LEHMANN, S. (2023) Fundamental structures in temporal communication networks. *Temporal Network Theory* (P. Holme & J. Saramäki eds). Cham: Springer International Publishing, 25–48.
6. SAQR, M. & LÓPEZ-PERNAS, S. (2022) The why, the what and the how to model a dynamic relational learning process with temporal networks. *Proceedings of the NetSciLA22 Workshop* (A. Garcia Castro, C. Lange, P. Lord and R. Stevens eds). Aachen, Germany: CEUR Workshop Proceedings.
7. TRØJELSGAARD, K. & OLESEN, J. M. (2016) Ecological networks in motion: micro-and macroscopic variability across scales. *Funct. Ecol.*, **30**, 1926–1935.
8. MEHDI HOSSEINZADEH, M., CANNATARO, M., HIRAM GUZZI, P. & DONDI, R. (2022) Temporal networks in biology and medicine: a survey on models, algorithms, and tools. *Netw. Model. Anal. Health Inf. Bioinform.*, **12**, 10.
9. HUYNH, N. & BARTHELEMY, J. (2022) A comparative study of topological analysis and temporal network analysis of a public transport system. *Int. J. Transp. Sci. Technol.*, **11**, 392–405.
10. SALAMA, M., EZZELDIN, M., EL-DAKHAKHNI, W. & TAIT, M. (2022) Temporal networks: a review and opportunities for infrastructure simulation. *Sustain. Resilient Infrastruct.*, **7**, 40–55.
11. BARRAT, A., BARTHÉLEMY, M. & VESPIGNANI, A. (2008) *Dynamical Processes on Complex Networks*. Cambridge, UK: Cambridge University Press.
12. BRAHA, D. & BAR-YAM, Y. (2009) Time-dependent complex networks: dynamic centrality, dynamic motifs, and cycles of social interactions. *Adaptive Networks: Theory, Models and Applications* (T. Gross & H. Sayama eds). Heidelberg: Springer Berlin, pp. 39–50.
13. PAN, R. K. & SARAMÄKI, J. (2011) Path lengths, correlations, and centrality in temporal networks. *Phys. Rev. E*, **84**, 016105.
14. LI, A., CORNELIUS, S. P., LIU, Y.-Y., WANG, L. & BARABÁSI, A.-L. (2017) The fundamental advantages of temporal networks. *Science*, **358**, 1042–1046.
15. BRAHA, D. & BAR-YAM, Y. (2006) From centrality to temporary fame: dynamic centrality in complex networks. *Complexity*, **12**, 59–63.
16. COSTA, E. C., VIEIRA, A. B., WEHMUTH, K., ZIVIANI, A. & PAULA COUTO DA SILVA, A. (2015) Time centrality in dynamic complex networks. *Adv. Complex Syst.*, **18**, 1550023.
17. BARABÁSI, A.-L. (2005) The origin of bursts and heavy tails in human dynamics. *Nature*, **435**, 207–211.
18. KARSAI, M., KASKI, K. & KERTÉSZ, J. (2012) Correlated dynamics in egocentric communication networks. *PLoS One*, **7**, e40612.
19. ALEDAVOOD, T., LEHMANN, S. & SARAMÄKI, J. (2015) Digital daily cycles of individuals. *Front. Phys.*, **3**, 73.
20. BAJARDI, P., BARRAT, A., NATALE, F., SAVINI, L. & COLIZZA, V. (2011) Dynamical patterns of cattle trade movements. *PLoS One*, **6**, e19869.
21. KOVANEN, L., KARSAI, M., KASKI, K., KERTÉSZ, J. AND SARAMÄKI, J. (2011) Temporal motifs in time-dependent networks. *J. Stat. Mech.*, **2011**, P11005.
22. LONGA, A., CENCETTI, G., LEPRI, B. & PASSERINI, A. (2022) An efficient procedure for mining egocentric temporal motifs. *Data Min. Knowl. Discov.*, **36**, 355–378.

23. GAUVIN, L., PANISSON, A. & CATTUTO, C. (2014) Detecting the community structure and activity patterns of temporal networks: a non-negative tensor factorization approach. *PLoS One*, **9**, e86028.

24. CSERMELY, P., LONDON, A., WU, L.-Y. & UZZI, B. (2013) Structure and dynamics of core/periphery networks. *J. Complex Netw.*, **1**, 93–123.

25. PEDRESCHI, N., BERNARD, C., CLAWSON, W., QUILICHINI, P., BARRAT, A. & BATTAGLIA, D. (2020) Dynamic core-periphery structure of information sharing networks in entorhinal cortex and hippocampus. *Netw. Neurosci.*, 4, 946–975.

26. PEDRESCHI, N., BATTAGLIA, D. & BARRAT, A. (2022) The temporal rich club phenomenon. *Nat. Phys.*, **18**, 931–938.

27. GALIMBERTI, E., BARRAT, A., BONCHI, F., CATTUTO, C. & GULLO, F. (2018) Mining (maximal) span-cores from temporal networks. *Proceedings of the 27th ACM International Conference on Information and Knowledge Management* (A. Cuzzocrea, J. Allan, N. W. Paton, D. Srivastava, R. Agrawal, A. Z. Broder, M. J. Zaki, K. Selçuk Candan, A. Labrinidis, A. Schuster & H. Wang eds). New York, NY, USA: Association for Computing Machinery, pp. 107–116.

28. SARAMÄKI, J. & MORO, E. (2015) From seconds to months: an overview of multi-scale dynamics of mobile telephone calls. *Eur. Phys. J. B*, **88**, 1–10.

29. GELARDI, V., FAGOT, J., BARRAT, A. & CLAIDIÈRE, N. (2019) Detecting social (in) stability in primates from their temporal co-presence network. *Anim. Behav.*, **157**, 239–254.

30. MASUDA, N. & HOLME, P. (2019) Detecting sequences of system states in temporal networks. *Sci. Rep.*, **9**, 1–11.

31. FOURNET, J. & BARRAT, A. (2014) Contact patterns among high school students. *PLoS One*, 9, e107878.

32. LUCAS, M., MORRIS, A., TOWNSEND-TEAGUE, A., TICHIT, L., HABERMANN, B. & BARRAT, A. (2023) Inferring cell cycle phases from a partially temporal network of protein interactions. *Cell Rep. Methods*, 3.

33. STEHLÉ, J., ET AL. (2011) High-resolution measurements of face-to-face contact patterns in a primary school. *PLoS One*, 6, e23176.

34. DARST, R. K., GRANELL, C., ARENAS, A., GÓMEZ, S., SARAMÄKI, J. & FORTUNATO, S. (2016) Detection of timescales in evolving complex systems. *Sci. Rep.*, 6, 39713.

35. SUGISHITA, K. & MASUDA, N. (2021) Recurrence in the evolution of air transport networks. *Sci. Rep.*, 11, 1–15.

36. LACASA, L., RODRIGUEZ, J. P. & EGUILUZ, V. M. (2022) Correlations of network trajectories. *Phys. Rev. Res.*, 4, L042008.

37. BAGROW, J. P. & BOLLT, E. M. (2019) An information-theoretic, all-scales approach to comparing networks. *Appl. Netw. Sci.*, 4, 1–15.

38. VALDANO, E., FERRERI, L., POLETTO, C. & COLIZZA, V. (2015) Analytical computation of the epidemic threshold on temporal networks. *Phys. Rev. X*, 5, 021005.

39. SATO, K., OKA, M., BARRAT, A. & CATTUTO, C. (2021) Predicting partially observed processes on temporal networks by Dynamics-Aware Node Embeddings (DyANE). *EPJ Data Science*, **10**, 22.

40. KIVELÄ, M., CAMBE, J., SARAMÄKI, J. & KARSAI, M. (2018) Mapping temporal-network percolation to weighted, static event graphs. *Sci. Rep.*, **8**, 1–9.

41. MELLOR, A. (2019) Event graphs: advances and applications of second-order time-unfolded temporal network models. *Adv. Complex Syst.*, **22**, 1950006.

42. SHANNON, C. E. (1949) Communication in the presence of noise. *Proc. IRE*, **37**, 10–21.

43. PERRA, N., GONÇALVES, B., PASTOR-SATORRAS, R. & VESPIGNANI, A. (2012) Activity driven modeling of time varying networks. *Sci. Rep.*, 2, 1–7.

44. SULO, R., BERGER-WOLF, T. AND GROSSMAN, R. (2010) Meaningful selection of temporal resolution for dynamic networks. *Proceedings of the Eighth Workshop on Mining and Learning with Graphs* (U. Brefeld, L. Getoor & S. A. Macskassy eds). New York, NY, USA: Association for Computing Machinery, pp. 127–136.

45. KRINGS, G., KARSAI, M., BERNHARDSSON, S., BLONDEL, V. D. & SARAMÄKI, J. (2012) Effects of time window size and placement on the structure of an aggregated communication network. *EPJ Data Sci.*, **1**:1–16.

46. Kivelä, M. & Porter, M. A. (2015) Estimating interevent time distributions from finite observation periods in communication networks. *Phys. Rev. E*, **92**, 052813.

47. Toth, D. J. A., Leecaster, M., Pettey, W. B. P., Gundlapalli, A. V., Gao, H., Rainey, J. J., Uzicanin, A. & Samore, M. H. (2015) The role of heterogeneity in contact timing and duration in network models of influenza spread in schools. *J. R. Soc. Interface*, **12**, 20150279.

48. Bureau of Transportation Statistics, Bureau of Transportation Statistics Website (2017).

49. Cattuto, C., Van den Broeck, W., Barrat, A., Colizza, V., Pinton, J.-F. & Vespignani, A. (2010) Dynamics of person-to-person interactions from distributed RFID sensor networks. *PLoS One*, **5**, e11596.

50. Génois, M., Zens, M., Oliveira, M., Lechner, C. M., Schaible, J. & Strohmaier, M. (2023) Combining sensors and surveys to study social interactions: a case of four science conferences. *Personal. Sci.*, **4**, 1–24.

51. Bai, C., Kumar, S., Leskovec, J., Metzger, M., Nunamaker Jr, J. F. & Subrahmanian, V. S. (2019) Predicting the visual focus of attention in multi-person discussion videos. *IJCAI* (S. Kraus ed). Macao, China: International Joint Conferences on Artificial Intelligence Organization, pp. 4504–4510.

52. Kumar, S., Bai, C., Subrahmanian, V. S. & Leskovec, J. (2021) Deception detection in group video conversations using dynamic interaction networks. *ICWSM* (A. Goel ed). Palo Alto, California, USA: AAAI Press, pp. 339–350.

53. Gauvin, L., Génois, M., Karsai, M., Kivelä, M., Takaguchi, T., Valdano, E. & Vestergaard, C. L. (2022) Randomized reference models for temporal networks. *SIAM Rev.*, **64**, 763–830.

54. Newman, M. (2018) *Networks*. Oxford, UK: Oxford University Press.

55. Battiston, F., Cencetti, G., Iacopini, I., Latora, V., Lucas, M., Patania, A., Young, J.-G. & Petri, G. (2020) Networks beyond pairwise interactions: structure and dynamics. *Phys. Rep.*, **874**, 1–92.

56. Battiston, F. et al. (2021) The physics of higher-order interactions in complex systems. *Nat. Phys.*, **17**, 1093–1098.